Microporous and Mesoporous Materials 181 (2013) 1–7

Contents lists available at ScienceDirect

Microporous and Mesoporous Materials

journal homepage: www.elsevier.com/locate/micromeso

Controlled release of ferulic acid from a hybrid hydrotalcite and its application as an antioxidant for human fibroblasts

Enrique Lima [a,*], Jorge Flores [b], Alejandra Santana Cruz [b], Gerardo Leyva-Gómez [c], Edgar Krötzsch [c]

[a] Instituto de Investigaciones en Materiales, Universidad Nacional Autónoma de México, Circuito exterior s/n, Cd. Universitaria, Del. Coyoacán, CP 04510 México D.F., Mexico
[b] Universidad Autónoma Metropolitana, Azcapotzalco, Av. San Pablo 180, Col. Reynosa Tamaulipas, 02200 México D.F., Mexico
[c] Laboratory of Connective Tissue, Centro Nacional de Investigación y Atención de Quemados, Instituto Nacional de Rehabilitación, México D.F., Mexico

ARTICLE INFO

Article history:
Received 23 April 2013
Received in revised form 20 June 2013
Accepted 8 July 2013
Available online 17 July 2013

Keywords:
Antioxidants
Hydrotalcite
Fibroblasts
Ferulic Acid

ABSTRACT

Ferulic acid anions were intercalated in a Zn–Al layered double hydroxide. The materials generated by this process were characterised structurally and tested in two important applications: as *in vitro* drug delivery agents in a system that mimics biological conditions, for which a mathematical model describing the drug delivery profile was created, and as antioxidants for human fibroblasts.

1. Introduction

Oxidative stress resulting from the imbalance between pro- and antioxidants has been implicated in several neurodegenerative disorders, such as Alzheimer's disease, and vitagenes [1]. In this sense, the use of antioxidants has been recognised as an important counter measure against conditions under which oxidative stress is generated. Among the plethora of naturally occurring compounds, phenolic acids have been given special attention [2,3]. The antioxidant properties of ferulic acid (FA) (4-hydroxy-3-methoxycinnamic acid) in particular have been well known since the 1970s [4]; FA acts as a scavenger against hydroxyl and peroxyl radicals [5]. Other physiological functions of FA have been explored (*i.e.*, antimicrobial, anti-inflammatory, anti-thrombosis, UV-protector and anticancer properties). Due to its many health benefits as well as its antioxidant and antimicrobial activity and low toxicity, FA has been approved as a food additive and used as a natural antioxidant in foods, beverages and cosmetics in Japan.

It is the phenolic –OH group in FA that transfers hydrogen to free radicals to provide the antioxidant effect [6]. Compared to that of other phenolic acids, the antioxidant effect of FA has been shown to be equivalent to that of lecithin as observed in the peroxidation of ghee [6].

The total antioxidant activities, expressed in TEAC (*i.e.,* total equivalent antioxidant capacity) values, of phenolic acids have been reported to rank as follows: ferulic > vanillic > syringic > caffeic > *m*-coumaric > protocatechuic > gentisic > *o*-coumaric [7].

With respect to radical-scavenging activity, it has been observed that the number of hydroxyl moieties attached to phenolic acids of the benzoic and cinnamic acid families dictates their radical-scavenging activities [8].

FA is one of the most abundant phenolic acids found in plants [9,10]; nevertheless, it is rarely found in its free form, usually occurring as an ester covalently linked to polysaccharides [11]. In reality, cellular delivery involving the transfer of drugs and bioactive molecules through the cell membrane into cells is a topic that has attracted much attention because of the inefficiency and difficulty of the transfer process. Therefore, the search for efficient and safe transport agents to deliver biomolecules and drugs remains a challenge for science. In this context, inorganic agents, mainly porous or laminated agents, show promising controlled-delivery properties [12] and are alternatives to viral carriers and organic cationic carriers. Porous materials are suitable for drug and gene delivery [13–15] because of the particular interactions that occur between drug materials inside the pores of such materials. These interactions frequently occur through dipoles and partially stabilise drugs in pores, protecting them until the hybrid materials reach cells.

A wide variety of porous materials have been proposed as hosts of organic molecules [16,17]. The most recurrent among these materials are mesoporous silica, zeolites, titanium oxide and layered double hydroxides (LDHs). LDHs, also known as hydrotalcite-like compounds (HTCs), are particularly suitable for this

* Corresponding author. Tel.: +52 (55) 5622 4640; fax: +52 (55) 5616 1371.
E-mail address: lima@iim.unam.mx (E. Lima).

1387-1811/$ - see front matter © 2013 Elsevier Inc. All rights reserved.
http://dx.doi.org/10.1016/j.micromeso.2013.07.014

application because of their good biocompatibility and potential capability for target delivery [18].

LDHs are materials consisting of positively charged layers separated by anions and water molecules. Their chemical composition is represented by the general formula $[M^{2+}_{(1-x)}M^{3+}_{x}(OH)_2]A^{n-}_{x/n}\cdot mH_2O$, where M^{2+} and M^{3+} are divalent and trivalent metal cations, respectively, and A^{n-} may be an exchangeable inorganic or organic anion. Due to this anionic exchange property, LDHs can be anionic carriers and be used instead of viral agents, which are often highly toxic to cells.

The LDH structure is reminiscent of that of brucite, where $Mg(OH)_6$ octahedral units share edges to form infinite $Mg(OH)_2$ layers. The structure of LDHs results from the partial isomorphic replacement of Mg^{2+} cations of brucite by Al^{3+} cations. As a consequence, an overall positive charge on the layers is created, which allows for the fine tuning of the material to suit specific applications by reducing or increasing the overall positive charge and thus the capacity for anions (anion exchange capacity, AEC), basicity and catalytic activity. Another interesting property of LDHs is the so-called memory effect: after relatively mild calcination, the layered structure collapses, but the layered double hydroxide structure can be regenerated after exposure to aqueous or organic solutions of anions [19,20]. This exchange reaction is regulated by the selectivity of the host for various counterions, the concentration and temperature [21]. In the case in which the counterions are organic anions with biological activity, the interlayer space behaves as a nanocontainer where these molecules are stored, protected, and later released under control by deintercalation. Thus, these intercalation compounds based on LDH can act as matrices or hosts for active molecules, yielding interesting hybrid nanocomposite materials [22]. Several pharmaceutically active drugs:antibiotics [23,24], anticarcinogens [25–27], cardiovasculars and anti-inflammatories [28], antihistamines [29], antihypertensives [30] and antifungals [31] have thus been intercalated into LDHs to obtain hybrid drug-inorganic matrix materials.

The objective of this study was to demonstrate the potential use of ferulic acid intercalated into a biocompatible ZnAl layered double hydroxide. Two *in vitro* studies were carried out to determine the viability of using this material as an antioxidant for human fibroblasts and also as a prolonged drug delivery system.

2. Experimental

2.1. Synthesis

The urea hydrolysis method was used to synthesise pure ZnAl–NO_3 ($Zn^{2+}/Al^{3+} = 2$) layered double hydroxide [32]. All reagents were purchased from Sigma–Aldrich. Briefly, $Zn(NO_3)_2{\cdot}6H_2O$ and $Al(NO_3)_3{\cdot}9H_2O$ were dissolved in CO_2-free distilled and deionised water at room temperature. Then, a mixture of urea and ammonium nitrate was added, and the mixture was magnetically stirred in a three-necked 500-mL round-bottom flask equipped with a reflux condenser at 90 °C for 10 h. The system was purged of CO_2 by bubbling argon gas for 1 h. The molar concentrations in the final solution were 0.335, 0.165, 1.65 and 1 mol L^{-1} for Zn^{2+}, Al^{3+}, urea and NH_4NO_3, respectively, resulting in a NO_3^-/urea molar ratio equal to 1.312. The white precipitate was centrifuged for 15 min, washed with hot deionised and CO_2-free water and finally dried at 120 °C for 12 h in an oven.

After the ZnAl–NO_3 LDH was prepared, the memory effect was used to produce an LDH containing intercalated FA (ZnAl–FA). Briefly, ZnAl–NO_3 LDH was first heat-treated in flowing N_2 (heating rate of 5 °C min^{-1}) to 500 °C, where it was maintained for 5 h to obtain the mixed oxide ZnAl(O). After cooling to room temperature, the mixed oxide (0.37 g) was suspended in a CO_2-free aqueous solution of ferulate sodium salt at room temperature under an argon atmosphere. The resulting suspension was magnetically stirred for 7 days. FA is poorly soluble in water; thus, to generate a soluble anionic species, an aqueous solution of ferulate anion was freshly prepared by adding 0.1 M NaOH to a 30-mL suspension containing 4.8 mmol of FA until the pH reached 9. The ZnAl–FA solid was then separated by centrifugation, washed several times with deionised water and dried in an oven at 80 °C overnight.

2.2. Materials characterisation

X-ray powder diffraction patterns were obtained using CuK_α radiation (λ = 1.54 Å) on a Philips X'Pert Pro instrument operating at 45 kV and 40 mA in the 2θ range of 4–80°, with a step size of 0.02° and step scan of 0.4 s.

Infrared spectra were recorded in the spectral window 4000–400 cm^{-1} using an FTIR Nicolet Magna IR 750 infrared spectrophotometer. Samples were diluted with KBr and handled as pellets.

Nitrogen adsorption isotherms were determined at −196 °C using a volumetric adsorption BELSORP apparatus (BEL Japan). Prior to the adsorption of N_2, all of the samples were outgassed at 90 °C for 12 h.

The morphology of the samples was studied with a SEM JEOL 7600 scanning electron microscope.

Solid-state ^{27}Al and ^{13}C magic angle spinning-nuclear magnetic resonance (MAS-NMR) experiments were performed on a Bruker Avance II spectrometer at frequencies of 104.2 and 100.58 MHz, respectively. ^{13}CP MAS-NMR spectra were acquired using a 4-mm cross-polarisation (CP) MAS probe spinning at a rate of 5 kHz. Typical ^{13}C CP MAS-NMR conditions for the ^1H-^{13}C polarisation experiment, included a $\pi/2$ pulse of 4 μs, contact time of 1 ms and delay time of 5 s. Chemical shifts were referenced to a solid shift at 38.2 ppm relative to TMS. ^{27}Al MAS-NMR spectra were acquired using short single pulses ($\pi/12$) and a delay time of 0.5 s. The samples were spun at 10 kHz, and the chemical shifts were referenced to an aqueous 1 M $AlCl_3$ solution.

2.2.1. In vitro studies

2.2.1.1. Drug release. Drug release studies were performed in a dialysis bag (the dialysis bag consisted of regenerated cellulose, 12,000–14,000 Da, 25-Å pore diameter, SERVA). Vessels were kept in a thermostatically controlled circulating water bath at 37.0 ± 0.5 °C with a rotational speed of 100 rpm. The dissolution medium was phosphate buffer with a pH of 7.5 (50 mM disodium hydrogen phosphate). The release studies were performed by placing 20 mg of ZnAl–FA in 50 mL of medium under sink conditions. Samples of 100 μL were withdrawn at predetermined intervals, followed by replenishment after each withdrawal with the same volume of fresh medium equilibrated at 37.0 ± 0.5 °C. Samples were appropriately filtered and analysed by UV spectrophotometry (Nanodrop 2000, Thermo Scientific, DE, USA) at λ_{max} = 310 nm according to a previously determined calibration curve (ranging from 5 to 150 μg/mL, $y = 0.007x + 0.003$, $r = 0.999$). The percentage released at each time point was expressed as a fraction of the total amount of FA. Drug release was monitored for 10 h; the FA concentration was reported as the average of 3 determinations. All recordings were within the range of the calibration curve.

2.2.1.2. Antioxidant activity in human cells. The procedure followed to measure antioxidant activity in human cells can be summarised in three steps: (i) *Antioxidant preparation*. LDH loaded with ferulic acid (ZnAl–FA) or control materials (ZnAl–NO_3, FA or a mixture of ZnAl–NO_3 plus FA) were dispersed in water at concentrations equivalent to 50 μM of FA. To prevent FA from being released from the LDH during the sterilisation procedure (autoclave), ZnAl-FA

was re-suspended in acetic acid 5 mM at pH = 3.2 and immediately administered to the cultures. Under these conditions, ZnAl–FA was stable and did not dissolve.

(ii) *Culture Cells*. Human fibroblast cultures were maintained in Dulbecco's Modified Eagle's Media (D-MEM; Gibco; Invitrogen, CA, USA) supplemented with 10% foetal bovine serum (Gibco), 2 mM L-glutamine (Gibco) and 100 U/mL penicillin–streptomycin (Gibco) in an incubator at 37 °C with 5% CO_2. Cells from the 6th passage were cultured on 5-well culture slides (Falcon, Becton Dickinson Labware, NJ, USA) at densities of 2.5×10^4 cells/cm^2 to obtain sub-confluent cultures, and they were incubated for 24 h. The cultures were then treated with 10 µl of either ZnAl–FA or the above-mentioned controls for 3 and 24 h and incubated under the conditions previously mentioned. To induce oxidative stress, a 500 µM H_2O_2 solution (10 µl) was added to every culture, and all cultures were incubated for an additional 4 h [33]. Cultures were washed twice with phosphate buffer saline (PBS), and changes in mitochondrial oxidant production were measured by incubating every culture for 15 min with 1 mL of 5 µM 3,8-phenanthridine diamine, 5-(69-triphenyl phosphonium hexyl)-5,6 dihydro-6-phenyl (MitoSOX Red staining, Invitrogen Corp., CA, USA) in PBS [34].

Cells were washed twice with PBS and fixed with 4% paraformaldehyde at 4 °C for 24 h. The slides were then mounted with Vectashield® mounting medium with DAPI (Vector Laboratories, Inc., CA, USA). MitoSOX™ exhibits fluorescence after oxidation by superoxide ion (excitation 510 nm, emission 580 nm), and DAPI exhibits an affinity for nucleic acids (excitation 360 nm, emission 460 nm). Images were recorded with a microscope (Axio Observer Z1; Carl Zeiss, Göttingen, Germany) fitted with a monochromatic high-speed camera (AxioCam camera Carl Zeiss).

Fluorescence densitometric evaluation was performed by digital image analysis by assessing 5 random cells in equivalent central fields for every culture using AxioVision digital image processing software (AxioVision 4.8.1.0, Carl Zeiss). All experiments were performed twice.

(iii) *Statistical analyses.* General differences in fluorescence proportion were assessed with a non-parametric Kruskal–Wallis analysis of variance (ANOVA). Group comparisons were made using Dunn's test. A specific comparison between the 3-h and 24-h treatments of FA and/or HT-FA was made by the Mann–Whitney Test. P values less than 0.05 were considered to be significant.

3. Results and discussion

3.1. Materials

The chemical compositions of ZnAl–NO_3 and ZnAl–FA are reported in Table 1. The chemical formulas show that FA anions are intercalated as monovalent species (carboxylate). Their X-ray diffraction patterns are compared in Fig. 1 and the cell parameters reported in Table 1. The position of peak (003) changes with the nature of the anions intercalated between the brucite-like layers. As a result of FA intercalation, the interlayer distance increases from 8.9 Å for ZnAl–NO_3 to 14.5 Å. As the layer thickness approaches 4.8 Å, the gallery height in ZnAl-FA becomes 9.7 Å, within the range previously reported for some phenolic anions [35]. A gallery height of 9.7 Å suggests that FA anions were arranged in the interlayer region as a monolayer with the main axis perpendicular to the layer plane of LDH. Furthermore, the composition of ZnAl–FA confirms that FA anions were intercalated as monovalent species, i.e., carboxylates.

Table 1
Chemical composition, and cell parameters of LDHs.

Sample	Chemical formulas	*a* (Å)	*c* (Å)
ZnAl–NO_3	$[Zn_{0.66}Al_{0.30}(OH)_2](NO_3)_{0.30}x0.50H_2O$	3.0857	26.7
ZnAl–FA	$[Zn_{0.66}Al_{0.30}(OH)_2](C_{10}H_9O_4)_{0.30}x0.55H_2O$	3.0656	43.5

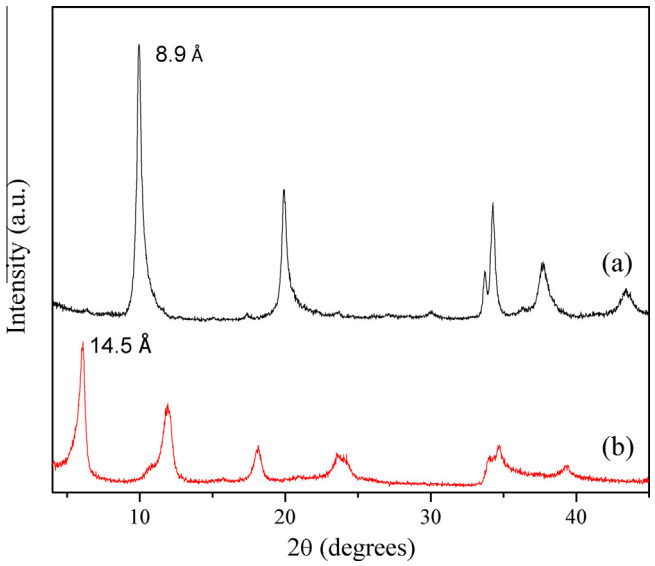

Fig. 1. XRD pattern of ZnAl–NO_3 (a) and ZnAl–FA (b). Peaks (003) were labelled with the corresponding interlayer distances.

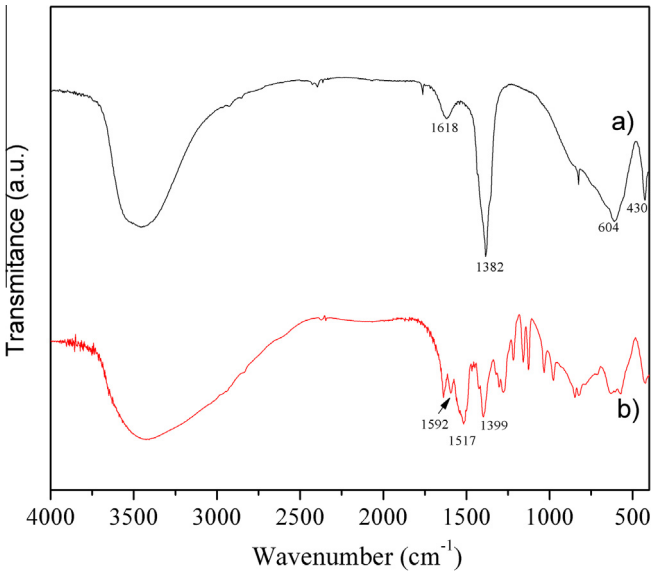

Fig. 2. Infrared spectra for ZnAl–NO_3 (a) and ZnAl–FA (b).

The FT-IR spectra of ZnAl–NO_3 and ZnAl–FA hybrid are compared in Fig. 2. For the ZnAl–NO_3 sample (Fig. 2a), the broad absorption band at approximately 3400–3500 cm^{-1} is assigned to the stretching frequency mode of O–H groups in the brucite-like layer and interlayer water. The absorption at 1618 cm^{-1} originates from the O–H bending vibration of hydroxyl groups. The strong absorption band at 1382 cm^{-1} is due to the stretching vibration of intercalated NO_3^- anions, and the bands at 604 and 430 cm^{-1} are ascribed to the lattice vibration modes attributed to M–O and O–M–O vibrations. Anionic exchange through the memory effect results in the complete disappearance of the NO_3^- band at 1382 cm^{-1}, and the antisymmetric and symmetric stretching modes of carboxylate groups observed at 1592 and 1399 cm^{-1}, respectively, show that ferulate anion has been intercalated,

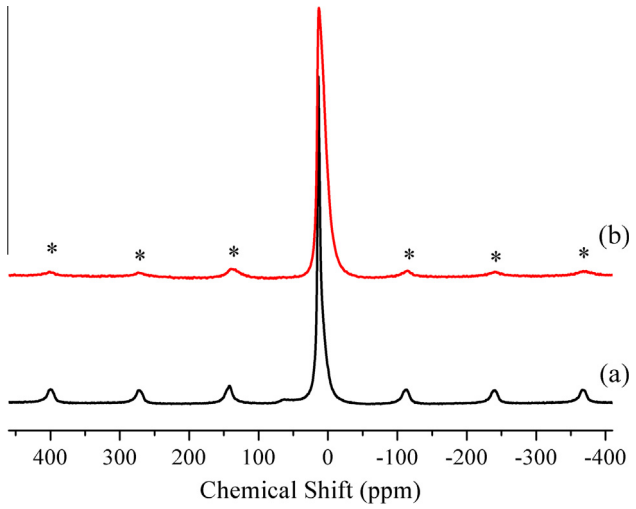

Fig. 3. ^{27}Al MAS NMR of ZnAl–NO_3 (a) and ZnAl–FA (b). * indicates spinning side bands (10 kHz).

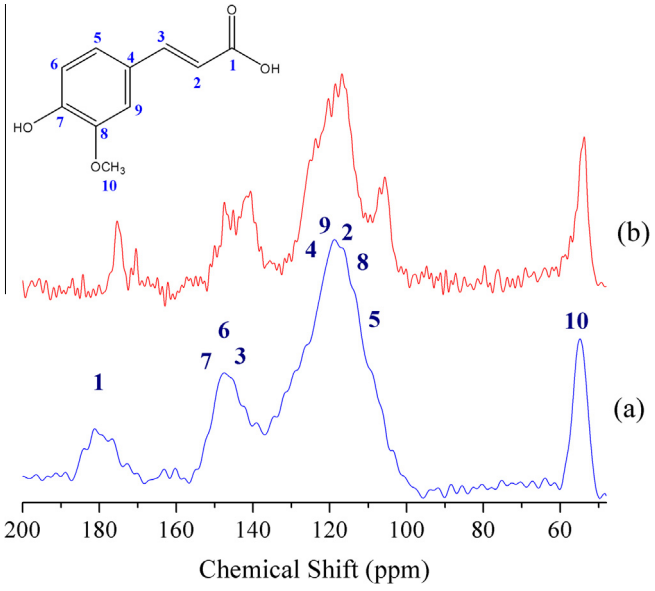

Fig. 4. ^{13}CP MAS NMR of sodium FA salt (a) and ZnAl–FA (b). Labelling of peaks in spectrum (a) corresponds to assignation o resonances according to numbering of carbons in structure of inset.

perhaps interacting through bonding hydrogen between oxygen from carboxylate and hydrogen from brucite-like layers. The absence of the band at 1704 cm^{-1} confirms that nitrate or carbonate species are not present in the ZnAl–FA sample, in line with the chemical composition of the solid. It can be concluded that the band near 1399 cm^{-1} is related to nitrates, but FA also shows two absorptions peaks due to stretching vibrations of O-methyl groups that could be included in this band. Finally, the very strong FT-IR band at 1517 cm^{-1} is assigned to C–C stretching vibration for both aromatic and propenoic acid [36]. Other infrared bands for the ZnAl–FA hybrid were not assigned in detail.

The ^{27}Al MAS-NMR spectra (Fig. 3) show a single resonance peak at 11 ppm for both the ZnAl–NO_3 and ZnAl–FA samples. The peak is notably broader in the sample containing FA than in the FA-free sample, suggesting that the relaxing behaviour of aluminium in LDH is modified by the high electronic density introduced by FA anions. In reality, it is possible that the carboxylate function is ionically bonded to the aluminium cations of the double hydroxide layers [37]. In this sense, ^{13}C CP MAS NMR spectra of Fig. 4 are relevant because they show some difference between the spectra of FA salt and FA intercalated in ZnAl LDH. The NMR peaks in both spectra are broad. On the one hand, the FA salt was prepared from pure FA, obtaining a solid poorly crystalline where ionic and dipolar interactions are present originating then broad resonance peaks. When FA anions are intercalated in the LDH, the resonance peaks became slightly finer but not enough to conclude on elimination or increasing dipolar interactions, maybe the decrease of broadness line is the consequence of the ordering of anions between the layers of LDH. Broad resonance peaks were grouped according to carbon numbering of structural drawn in the inset of Fig. 4. In reality, the resonance due to carbon C1 goes to upper field when the FA is intercalated in the LDH confirming that the intercalation of FA anions occurs trough an interaction of carboxylate function with the brucite-like layers.

Fig. 5 compares SEM images of the HT sample before and after FA intercalation. Significant differences are observed: in the samples nitrated before intercalation, the primary HT nanoparticles show great cohesion, leading to the formation of large particles with a "stone-like" morphology. When FA anions are present instead of nitrates, the particles became smoother with good crystallinity to yield the 'rose-petal' morphology characteristic of hydrotalcite materials, which indicates that the gradual rehydration of mixed oxide (calcined ZnAl–NO_3) in the presence of FA anions allows for the lamination of the material to be better organised.

Changes in morphology alter the porosity of materials, mainly at the macroporous level. To verify that the mesoporosity of the materials was not altered, the N_2 isotherms of the materials were determined. Fig. 6 shows that the nitrated sample yielded a reversible nitrogen isotherm (Fig. 6a) classified as type II according to the IUPAC classification [38]. A narrow hysteresis loop appeared at high relative pressure. It is clear that the HT platelets are rigid, and the packing arrangement formed a macroporous aggregate,

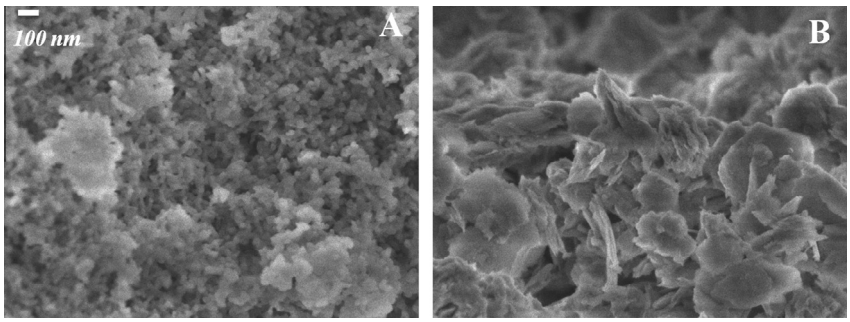

Fig. 5. SEM images of ZnAl–NO_3 (A) and ZnAl–FA (B). Scale bar is valid for both images.

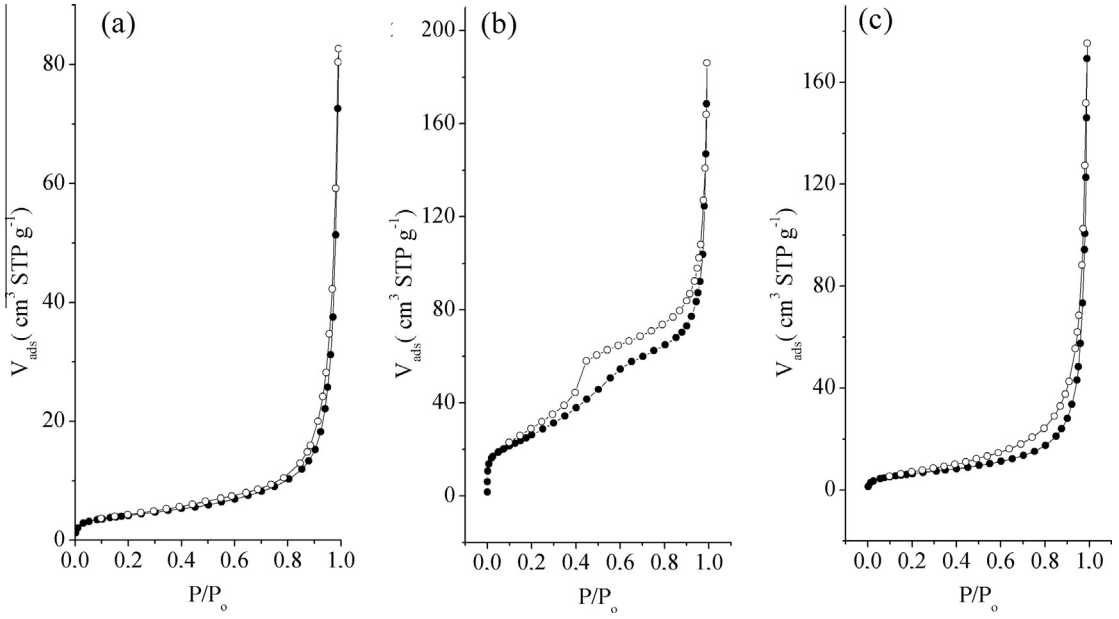

Fig. 6. N_2 adsorption (fill circles)-desorption (empty circles) of ZnAl–NO_3 (a), ZnAl–NO_3 thermal treated at 500 °C (b) and ZnAl–FA (c). Previous to adsorption samples were outgased at 90 °C.

as evidenced by the SEM micrographs. This material possessed an average porous diameter and specific surface area of 32.3 nm and 15 $m^2 g^{-1}$, respectively, which correspond to a platelet thickness of approximately 50 nm. With thermal treatment, the delamination of HT occurs, leading to a mesoporous material (Fig. 6b). This isotherm is type IV according to the IUPAC classification. An H1 hysteresis loop is relatively narrow with the adsorption and desorption branches nearly parallel, which is related to the compact packing of small particles and narrow pore-size distributions. The results show that the specific surface area was high (97 $m^2 g^{-1}$) and the average pore size relatively small (11.9 nm). This high surface area is important because it provides greater access to intercalation of FA anions. When the intercalation is completed, a type-II isotherm is once again obtained (Fig. 6c). The specific surface area is again low (23 $m^2 g^{-1}$) and the average pore diameter relatively large (44 nm).

3.2. Prolonged drug delivery

The profiles demonstrating the diffusion of FA and drug release from ZnAl–FA in 50 mM phosphate buffer at pH 7.5 are compared in Fig. 7. It is evident that the release profile of FA is lower for ZnAl–FA than the drug diffusion.

The release profile of ZnAl–FA shows that 18% of the drug was released after 32 min, 34% after 1 h, 60% after 2 h, 86% after 4 h and 98% after 8 h. This difference is probably due to the drug release mechanism of the intercalating molecule because ferulic acid release from ZnAl–FA occurs through the exchange between FA ions [39] and HPO_4^{2-} and $H_2PO_4^-$ (it readily dissociates from Na_2HPO_4 at pH 7.5). A burst effect was observed in the matrix evaluated during the first two hours, followed by a slow release from the second to the tenth hour. The burst effect is due to the release of the intercalated ions. The second slow-release stage can be attributed to the release of FA ions from deeper interlayer sites (the effective distance to diffuse up to the edges reduces the release rate) together with a possible increase in the rigidity of the layers. This rigidity mechanism is explained [40,41] by the reduction of the interlayer distance due to the exit of larger anions and the entry of smaller ions, a gradual phenomenon. This

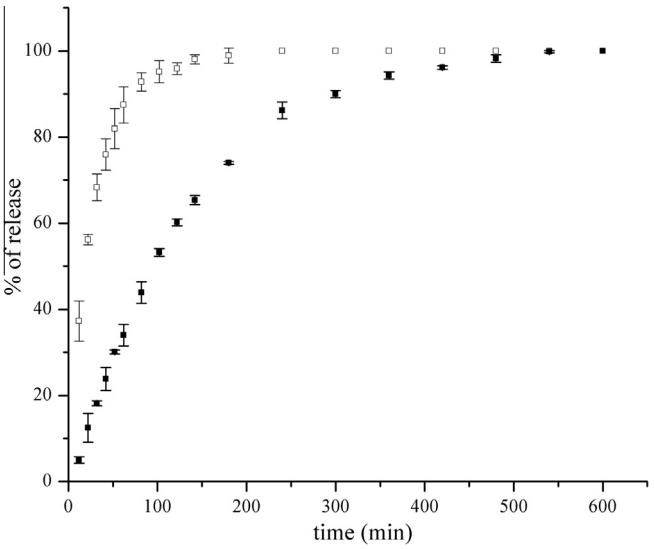

Fig. 7. Release profile of FA from ZnAl–FA (-■-) compared to diffusion profile recorded for FA (-□-) in 50 mM phosphate buffer at pH 7.5. Error bars represent standard deviation.

explanation is based on the rigidity properties of the matrix according to the classification of LDHs as a class-II material, as reported by Solin [42]. Thus, it is possible to also control the drug release rate by modifying the effective transit distance in the layer.

With the aim of investigating the precise release mechanism of the drug, several mathematical models were used to make approximations of different kinetics [43] (Table 2). The diffusional exponent (n) of the Ritger–Peppas kinetic model [44] was evaluated, and an increase in the value of the correlation coefficient can be observed as the exponent's value decreases, indicating that the release rate of the drug is time-dependent ($r = 0.812$) according to a zero-order mechanism. Then, when the data obtained using a value $n = 0.5$ were compared with the profile adjusted to a Higuchi mechanism, a higher value of the correlation coefficient was

Table 2
Mathematical model fitting of ZnAl–FA release data.

Equations		Linear regression
$Mt/M_\infty = 1 - e^{-Kt}$	First order	$y = -0.003x + 0.009$ $r = 0.997$
$Mt/M_\infty = 1 - e^{-Kt\ 0.65}$	Ionic exchange (Bhaskar)	$y = -0.029x + 0.227$ $r = 0.984$
$Mt/M_\infty = Kt^n$	$n = 0.5$ (Higuchi 0–60% release)	$y = 7.244x - 21.78$ $r = 0.994$
	$n = 0.5$	$y = 4.792x - 1.716$ $r = 0.933$
	$n = 0.6$	$y = 2.353x + 7.887$ r = 0.912
	$n = 0.7$	$y = 1.178x + 14.77$ $r = 0.888$
	$n = 0.8$	$y = 0.597x + 19.95$ $r = 0.863$
	$n = 0.9$	$y = 0.305x + 23.99$ $r = 0.838$
	$n = 1.0$	$y = 0.156x + 27.24$ $r = 0.812$

observed in the latter (0.933 vs. 0.994), verifying the existence of an important diffusion mechanism that affects the release of the drug. Because it has been reported in various studies that the ion exchange mechanism makes a significant contribution to the drug release rate [45,46], in this study, a correlation coefficient value less than the greatest value obtained for the models used was achieved (0.984 > 0.98); nevertheless, the coefficient does fit the data obtained, which means that the predominant mechanism is that of first-order kinetics and is associated with a concentration-dependent release of the drug. Therefore, the release mechanism of FA from LDH is explained by a concentration-dependent diffusion mechanism related to time as well as ion exchange (in fact, this ion exchange mechanism may provide the concentration gradient required for release). In summary, ZnAl–FA is a prolonged-release system that provides more than 98% of the drug after 8 h compared to FA diffusion, which provides the same amount of the drug in 2.36 h.

3.3. Antioxidant Activity

The fibroblast cultures treated with ZnAl–FA LDH and the controls exhibited a fusiform morphology, with normal vacuolisation as well as integral nuclear and cytoplasmic membranes (data not shown). On the other hand, after incubation in the presence of H_2O_2, fibroblasts exhibited higher MitoSOX cytoplasmic staining

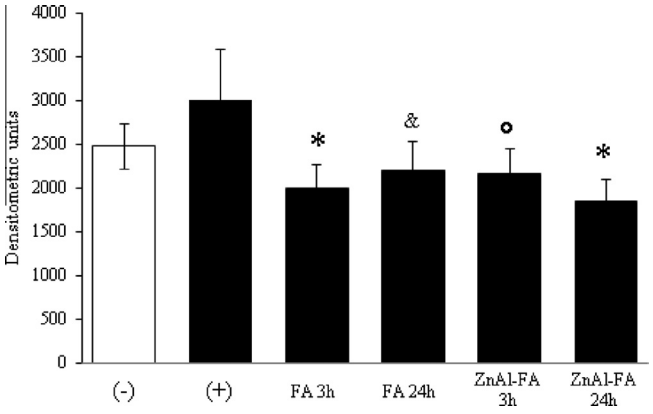

Fig. 9. *MitoSOX fluorescence evaluation.* Image densitometric analysis was performed to 5 individual cells from every culture in an experiment performed by duplicate. (−) Fibroblasts without any treatment, this is the basal cell oxidation, (+) Fibroblasts treated only with H_2O_2, this is the ROS induction, FA = ferulic acid, ZnAl–FA = composite of hydrotalcite-ferulic acid. Significant differences were observed when positive control (+) was compared with FA or ZnAl–FA. Control *vs.* FA 3 h or ZnAl–FA 24 h $^{*}p = 0.001$, *vs.* FA 24 h $^{\&}p = 0.05$ and *vs.* ZnAl–FA 3 h $^{\circ}p = 0.01$. Error bars represent standard deviation.

than untreated cultures or controls (Fig. 8a and b). It is remarkable that even after washing, the ZnAl–FA-treated cultures still showed HT particles (arrows in Fig. 8e and f). The 3-h and 24-h treatments with either FA or ZnAl–FA significantly prevented reactive oxygen species (ROS) production (Fig. 8c–f). A relevant result is that after 24 h of treatment with ZnAl–FA, cells showed the lowest MitoSOX fluorescence (Fig. 9). When comparing cells treated with ZnAl–FA (24 h) against cells treated with ZnAl–FA for 3 h or FA for 24 h, a statistically significant difference was observed ($p = 0.013$ and $p = 0.018$, respectively).

It is clear that FA and ZnAl–FA reduced intracellular ROS production, with a particular decrease in the induced superoxide ion evidenced by MitoSOX staining, where treatment with ZnAl–FA for 24 h showed lower fluorescence levels than that with FA at any time or that with ZnAl–FA at 3 h. This behaviour may be associated with FA exhaustion or to the rate of FA release from the ZnAl–FA composite. Previously, it was shown that after 3 h, FA release was approximately 70% of the total, as indicated in the section regarding prolonged drug release (Fig. 7).

ROS have been considered mainly to be cytotoxic metabolic byproducts; high levels of ROS will signal the initiation of senescence and apoptosis, and under the highest levels of cellular ROS,

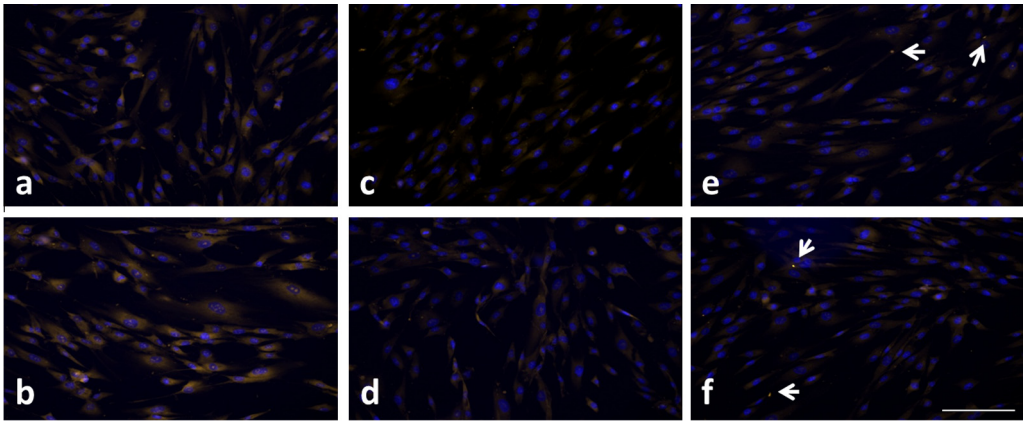

Fig. 8. *Assessment of superoxide ion formation.* Fibroblast cultures were untreated (a and b) or treated with FA for 3 h and 24 h (c and d) or ZnAl–FA for 3 h and 24 h (e and f). ROS were induced with 500 μM H_2O_2 for 4 h, except in (a); superoxide ion was evidenced by MitoSOX Red staining. LDH particles exhibited autofluorescence (arrows in e and f). Bar = 50 μm.

cellular components show irreversible damage. Otherwise, low levels of mitochondrial ROS production are required to regulate survival, proliferation and differentiation *via* induction of different intracellular pathways, such as phosphoinositide-3-kinase or the fork head box O transcription factor (FOXO), among others [47]; therefore, it is important to regulate intracellular ROS levels through antioxidant strategies. FA acts not only as a free-radical scavenger. Studies of neuronal and glial cells have shown that a ferulic acid derivative has a cytoprotective function related to its ability to induce the vitagene family. Vitagenes are a group of genes induced by stress that are involved in preserving cellular homeostasis. Oxidative stress is one important way in which vitagenes are induced. The product of one such gene, the heme oxygenase (HO)-1 enzyme, arises in skin fibroblasts and keratinocytes exposed to UVA irradiation and has been demonstrated to play a cytoprotective role [33]. Thus, the protective effect exhibited by FA against H_2O_2-induced oxidative damage highlights its potential use in the prevention of oxidative-stress-mediated skin damage.

4. Conclusion

Ferulic acid ions were successfully intercalated into a ZnAl layered double hydroxide (LDH) by exploiting to the memory effect of LDHs. FA ions incorporate into the LDHs produced in this study, where the main axis of the LDHs lay perpendicular to the brucite-like layers. LDH significantly prolonged the release of ferulic acid relative to the diffusion of ferulic acid in a dialysis bag. FA protected by LDH provides more than 98% of the drug after 8 h, longer than the 2.36 h required for ferulic acid diffusion to deliver the same amount. The potential use of FA intercalated into LDH as an efficient antioxidant of human fibroblasts was demonstrated. Pure FA as well as FA protected by LDH significantly reduced the production of intracellular reactive oxygen species. The diminution of the induced superoxide ion in particular deserves special attention. The antioxidant activity was observed for periods as long as 24 h when FA was protected by LDH.

Acknowledgments

Thanks are due to CONACYT for Grant 128299. We gratefully acknowledge G. Cedillo and A. Tejeda for their technical assistance.

References

[1] W.R. Markesbery, Biol. Med. 23 (1997) 134–147.
[2] H. Schroeter, R.J. Williams, R. Matin, L. Iversen, C.A. Rice-Evans, Free Radical Biol. Med. 29 (2000) 1222–1233.
[3] E. Graf, Free Radical Biol. Med. 13 (1992) 435–448.
[4] K. Yagi, N. Ohishi, J. Nutr. Sci. Vitaminol. 25 (1979) 127–130.
[5] J. Kanski, M. Aksenova, A. Stoyanova, D.A. Butterfield, J. Nutr. Biochem. 13 (2002) 273–281.
[6] S. Gupta, P.S. Sukhija, I.S. Bhatia, Milchwissenschaft 34 (1979) 205–206.
[7] C.A. Rice-Evans, N.J. Miller, G. Paganga, Free Radical Biol. Med. 20 (1996) 933–956.
[8] M. Karamaæ, A. Kosiñska, R.B. Pegg, Pol. J. Food Nutr. Sci. 14 (2005) 165–170.
[9] P.A. Kroon, C.B. Faulds, P. Ryden, J.A. Robertson, G.J. Williamson, Agric. Food Chem. 45 (1997) 661–667.
[10] J.P.N. Rosazza, Z. Huang, L. Dostal, T. Volm, B. Rousseau, J. Ind. Microbiol. 15 (1995) 457–471.
[11] M.M. Smith, R.D. Hartley, Carbohydr. Res. 118 (1983) 65–80.
[12] Q. Wang, D. O'Hare, Chem. Rev. 112 (2012) 4124–4155.
[13] Z. Lu, M.D. Prouty, Z. Guo, V.O. Golub, C.S.S.R. Kumar, Y.M. Lvov, Langmuir 21 (2005) 2042–2050.
[14] Y. Lu, Y. Zhao, L. Yu, L. Dong, C. Shi, M.J. Hu, Y.J. Xu, L.P. Wen, S.H. Yu, Adv. Mater. 22 (2010) 1407–1411.
[15] J. Zhu, S. Wei, S.B. Rapole, Q. Wang, Z. Luo, N. Haldolaarachchige, D.P. Young, Z. Guo, Environ. Sci. Technol. 46 (2012) 977–985.
[16] H. Laguna, S. Loera, I.A. Ibarra, E. Lima, M.A. Vera, V. Lara, Microporous Mesoporous Mater. 98 (2007) 234–241.
[17] Z. Xu, G.Q. Lu, Pure Appl. Chem. 78 (2006) 1771–1779.
[18] M.H. Kim, D.H. Park, J.H. Yang, Y.B. Choy, J.H. Choy, Int. J. Pharm. 444 (2013) 120–127.
[19] O. Meyer, F. Roessner, R.R.A. Rakoczy, R.W. Fischer, ChemCatChem 2 (2010) 314–321.
[20] J.B. Swadling, J.L. Suter, H.C. Greenwell, P.V. Coveney, Langmuir 298 (2013) 1573–1583.
[21] S. Miyata, Clays Clay Miner. 31 (1983) 305–311.
[22] J.-H. Choy, J.-M. Oh, T.T. Biswick, J. Mater. Chem. 19 (2009) 2553–2563.
[23] L. Tammaro, U. Costantino, A. Bolognese, G. Sammartino, G. Marenzi, A. Calignano, S. Teté, F. Mastrangelo, L. Califano, V. Vittoria, Int. J. Antimicrob. Agents 29 (2007) 417–423.
[24] M. Trikeriotis, D.F. Ghanotakis, Int. J. Pharm. 332 (2007) 176–184.
[25] J.-M. Oh, M. Park, S.-T. Kim, J.-Y. Jung, Y.-G. Kang, J.-H. Choy, J. Phys. Chem. Solids 67 (2006) 1024–1027.
[26] Z. Wang, E. Wang, L. Gao, L. Xu, J. Solid State Chem. 178 (2005) 736–741.
[27] S.-J. Choi, J.-M. Oh, J.-H. Choy, J. Phys. Chem. Solids 69 (2008) 1528–1532.
[28] A.I. Khan, L. Lei, A.J. Norquist, D. O'Hare, Chem. Commun. (2001) 2342–2343.
[29] S.H. Hussein-Al-Ali, M. Al-Qubaisi, M.Z. Hussein, M. Ismail, Z. Zainal, M.N. Hakim, Int. J. Mol. Sci. 13 (2012) 5899–5916.
[30] H. Zhang, K. Zou, S. Guo, X. Duan, J. Solid State Chem. 179 (2006) 1792–1801.
[31] C. Liu, W. Hou, L. Li, Y. Li, S. Liu, J. Solid State Chem. 181 (2008) 1792–1797.
[32] A. Inayat, M. Klumpp, W. Schwieger, Appl. Clay Sci. 51 (2011) 452–459.
[33] V. Calabrese, S. Calafato, E. Puleo, C. Cornelius, M. Sapienza, P. Morganti, C. Mancuso, Clin. Dermatol. 26 (2008) 358–363.
[34] C.M. Quinzii, L.C. López, J. Von-Moltke, A. Naini, S. Krishna, M. Schuelke, L. Salviati, P. Navas, S. DiMauro, M. Hirano, FASEB J. 22 (2008) 1874–1885.
[35] M. Meyn, K. Beneke, G. Lagaly, Inorg. Chem. 29 (1990) 5201–5207.
[36] S. Sebastiana, N. Sundaraganesana, S. Manoharanb, Spectrochim. Acta Part A 74 (2009) 312–323.
[37] C. Rossi, A. Schoubben, M. Ricci, L. Perioli, V. Ambrogi, L. Latterini, G.G. Aloisi, A. Rossi, Int. J. Pharm. 295 (2005) 47–55.
[38] K.S.W. Sing, D.H. Everett, R.A. Haul, L. Moscou, R.A. Pieorotti, J. Rouquerol, T. Siemienniewska, Pure Appl. Chem. 67 (1985) 603.
[39] V. Ambrogi, L. Perioli, M. Ricci, L. Pulcini, M. Nocchetti, S. Giovagnoli, C. Rossi, Microporous Mesoporous Mater. 115 (2008) 405.
[40] V. Ambrogi, G. Fardella, G. Grandolini, L. Perioli, Int. J. Pharm. 220 (2001) 23–32.
[41] U. Costantino, V. Ambrogi, M. Nocchetti, L. Perioli, Microporous Mesoporous Mater. 107 (2008) 149–160.
[42] S.A. Solin, in: M.S. Dresslhaus (Ed.), Intercalation in Layered Materials, Plenum Press, New York, 1986.
[43] L. Perioli, T. Posati, M. Nocchetti, F. Bellezza, U. Constantino, A. Cipiciani, Appl. Clay Sci. 53 (2011) 374–378.
[44] P. Ritger, N.A. Peppas, J. Controlled Release 5 (1987) 37–42.
[45] T. Ngawhirunpat, E. Goegebakan, S. Duanjit, P. Akkaramongkolporn, M. Kumpugdee-Vollrath, Int. J. Pharm. Pharm. Sci. 2 (2010) 107–112.
[46] R. Bhaskar, R.S.R. Murthy, B.D. Miglani, K. Viswanathan, Int. J. Pharm. 28 (1986) 59–66.
[47] M. Zhou, A. Xu, P.K.H. Tam, K.S.L. Lam, B. Huang, Y. Liang, I.-K. Lee, D. Wu, Y. Wang, PLoS One (2012) 7–12.